Investigation of Structural and Electrical Properties of $(Bi_2O_3)_{1-x-y}(CeO_2)_x(Eu_2O_3)_y$ Electrolytes for Solid Oxide Fuel Cells

Y. Islek[a,*], M. Kasikci Ozen[a], R. Kayali[a] and M. Ari[b]

[a]Department of Physics, Faculty of Science and Letters, Nigde Omer Halisdemir University, Nigde, Turkey

[b]Department of Physics, Faculty of Science, Erciyes University, Kayseri, Turkey

(Received November 27, 2017; in final form March 5, 2019)

In the present study, CeO_2 and Eu_2O_3 doped Bi_2O_3 composite materials for solid oxide fuel cells were investigated. $(Bi_2O_3)_{1-x-y}(CeO_2)_x(Eu_2O_3)_y$ ternary systems ($x = 0.01$, 0.03, 0.05, 0.07, 0.09, 0.11 and $y = 0.11$, 0.09, 0.07, 0.05, 0.03, 0.01 dopant concentrations) were fabricated at different temperatures (650, 700, 750, and 800 °C) using conventional solid-state synthesis techniques. Characterization of these electrolyte samples were carried out by X-ray powder diffraction, differential thermal analysis/thermal gravimeter, and the four-point probe technique measurements. X-ray powder diffraction measurements showed that nearly all the samples have $\alpha+\beta+\gamma$ phase except the samples with tetragonal β-phase sintered at 700, 750 °C and 750, 800 °C with the dopant ratios ($x = 0.07$, $y = 0.05$) and ($x = 0.09$, $y = 0.03$), respectively. Four-point probe technique measurements showed that the measured ionic conductivity of the stable samples vary in the range 1.05×10^{-1}–4.76×10^{-1} S/cm. Additionally, the activation energy values of the samples were calculated with the help of the Arrhenius equation adapted to the $\log\sigma$ graphics versus $1000/T$ varying in the range 0.7799–0.8746 eV. This result shows that there is a good relationship between the activation energy values and conductivity values.

DOI: 10.12693/APhysPolA.135.347

PACS/topics: solid state ceramic technique, activation energy, electrical conductivity, electrolyte, Arrhenius

1. Introduction

In recent years, fuel cells have been widely studied as very efficient electrochemical energy conversion devices due to their high-energy conversion efficiency, low system cost, high power density, environmental compatibility, very low pollution, as only operational byproduct is water resulting from combustion of hydrogen used as fuel [1–3]. Fuel cells are classified according to the type of electrolyte and fuel used in their construction and run, respectively and solid oxide fuel cells (SOFCs) have much greater fuel flexibility and the highest energy conversion efficiency with heat recovery. They generate electricity by electrochemical reaction of hydrogen and oxygen injected separately on anode and cathode electrodes of the cell with a solid ceramic electrolyte in the middle [4]. One of the most important components of a SOFC is electrolyte. Oxide-ion conducting solid electrolytes used in SOFCs, are also used in oxygen sensor and oxygen pumps [5, 6].

Electrolytes based on stabilised ZrO_2 are electrolytes used commonly in SOFCs and their operating temperature is in the range of 750–1000 °C [7]. High operating temperature in SOFCs causes undesirable high cost reactions between its metallic components [8]. Therefore, many researchers have focused on Bi_2O_3-based electrolytes operating in a lower temperature range (600–800 °C) [9, 10]. On the other hand, bismuth(III) oxide (Bi_2O_3) is an important functional material. Bi_2O_3-based electrolytes are used more in the SOFC and oxygen sensor applications for also exhibiting high ionic conductivity more than the zirconium-based electrolyte at the same temperature [10, 11].

Bi_2O_3 has six polymorphic phases, such as α-Bi_2O_3 (monoclinic), β-Bi_2O_3 (tetragonal), γ-Bi_2O_3 (cubic, bcc), δ-Bi_2O_3 (cubic, fcc), ε-Bi_2O_3 (orthorhombic) and ω-Bi_2O_3 (triclinic). α, β, γ, and δ-phases have been widely studied in SOFCs in order to achieve high ionic conducting electrolytes [12–14]. The face-centered cubic (fcc) δ- Bi_2O_3 phase has stable fluoride type structure and exhibits the highest oxygen ionic conductivity among all bismuth oxide phases in SOFCs [15, 16]. The tetragonal β-Bi_2O_3 phase and the body centered cubic (bcc) γ-Bi_2O_3 phase metastable structure show good oxygen ionic conductivity property [17]. Therefore, in order to preserve high conductivity properties of δ-Bi_2O_3, β-Bi_2O_3 and γ-Bi_2O_3 phases, bismuth oxide based electrolytes can be more stabilized by addition of rare earth elements such as Ho, Dy, Er, Tb, Tm, Eu, and Ce into pure Bi_2O_3 [18–21]. Many of the researchers have investigated crystal structures, stabilities, and conductivities of the bismuth based binary [17, 22–26] and ternary [27–30] ceramic electrolytes obtained doping different earth-rare elements.

In this study, we first have prepared 6 different powder groups mixing CeO_2, Eu_2O_3 powders with the percentages ($x = 0.01$, 0.03, 0.05, 0.07, 0.09, 0.11, $y = 0.11$, 0.09, 0.07, 0.05, 0.03, 0.01) keeping the

*corresponding author; e-mail: ymeric@ohu.edu.tr

percentage of Bi_2O_3 constant (0.88). Then, each of these 6 group powders have been divided into 4 parts and each of these 4 powders have been sintered in an high temperature oven at 4 different temperatures (650, 700, 750, and 800 °C) for 48 h by solid-state synthesis technique (SST). Hence, we have fabricated totally 24 $(Bi_2O_3)_{1-x-y}(CeO_2)_x(Eu_2O_3)_y$ ternary solid electrolyte samples. We have performed the characterization of the samples by X-ray powder diffraction (XRD), differential thermal analysis/thermal gravimeter (DTA/TGA), and four-point probe techniques (FPPT). After completing the characterization of the sample, we have selected 4 samples, two of which are group A4 and the other two are group A5, since they have the best stable and high conductive properties. Finally, we have discussed their properties in detail.

2. Experimental procedures

2.1. Sample preparations

We synthesized totally 24 $(Bi_2O_3)_{1-x-y}(CeO_2)_x(Eu_2O_3)_y$ ternary system samples using bismuth(III) oxide (Bi_2O_3, purity 99.99%, Alfa Aesar), cerium(II) oxide (CeO_2, purity 99.99 %, Alfa Aesar), and europium(III) oxide (Eu_2O_3, purity 99.99 %, Alfa Aesar) as precursor composite materials. To do this, firstly the powders of CeO_2 and Eu_2O_3 with the percentages (x = 0.01, 0.03, 0.05, 0.07, 0.09, 0.11 and y = 0.11, 0.09, 0.07, 0.05, 0.03, 0.01), respectively and Bi_2O_3 with constant percentage (0.88) were weighed, and then six powders were obtained mixing them. Each of these six different powders were grounded in an agate and they were labelled as A1, A2, A3, A4, A5, and A6. Then, all the samples were annealed at 600 °C for 24 h in an alumina crucible for preheating process. After this process, these powders were again homogeneously mixed by grinding in an agate mortar and then each of the powder corresponding to each of six labelled powders were divided into 4 parts. Finally, each of these 4 powders corresponding to each of the six group was synthesized in a ceramic crucible at 650, 700, 750, and 800 °C for 48 h, respectively. By this way 24 different powder mixtures were prepared. The prepared powder of each sample was divided into two parts. First parts of these powders were used for XRD, DTA, and TGA measurements. The second parts were pressed in a mold of 10 mm diameter and 2 mm thickness under pressure (10 MPa) to obtain a disk shaped pellet and then these pellets were sintered at 700 °C for 10 h. These pellets were used for FPPT measurements.

2.2. X-ray diffraction analyses

XRD measurements were carried out for the determination of the crystal structures of the samples, using a Bruker AXS D8 Advance, equipped with a copper X-ray source (λ = 1.544 Å), and a monochromatic eliminating K_α radiation. The measurements were carried out varying 2θ from 10° to 90°, scanning with a step of 0.002°/min.

2.3. Thermal analyses

The thermal behavior of the powder samples (20–50 mg) were determined by TGA/DTA thermal analysis by means of the Diamond TG/ DTA-Perkin Almer Marck device in the temperature range of 25–800 °C in an alumina crucible.

2.4. Electrical measurements

Electrical conductivities of the samples were measured using FPPT homemade system. The temperature changes of the samples heated in a controllable Nabertherm mark furnace were determined using a 0.5 mm standard K type thermocouple. All of the electrical measurements were taken by using Data Acquisition Control System integrated with a PC, interface card IEEE-488.2, multi meter with scanning card (Keithley 2700, 7700-2), programmable power supply (Keithley 2400), and computer program written for this purpose. The obtained data was used to plot the Arrhenius conductivity.

3. Results

3.1. XRD measurement results

Table I shows phase composition of 24 $(Bi_2O_3)_{1-x-y}(CeO_2)_x(Eu_2O_3)_y$ ternary system samples with different percentages of CeO_2 and Eu_2O_3 and synthesized at four different temperatures (650, 700, 750, and 800 °C) obtained from XRD measurements.

XRD measurement results presented in Table I showed that nearly all of the samples have $\alpha+\beta+\gamma$ phase except two samples corresponding A4 group synthesized at 700, 750 °C and the other two samples corresponding to A5 group synthesized at 750, 800 °C. These four samples have the most β-stable crystal structures compared to the others. Therefore these samples were submitted to the measurement of electrical properties.

Figure 1 shows the comparisons of the XRD patterns of the A4 sample synthesized at 700 and 750 °C for 48 h. As can be seen in Fig. 1, these XRD patterns show that the crystal structure of samples belong to a tetragonal type of the β-Bi_2O_3 phase. According to this result, the synthesizing temperature change plays an important role in the formation of metastable tetragonal β-Bi_2O_3 phase for A4 sample. Figure 2 shows the comparisons of the XRD patterns of the A5 sample synthesized at 750 and 800 °C for 48 h. As shown in this figure, XRD patterns of the A5 sample have quite similar properties compared to A4 sample. From this figure, it is observed that the A5 sample synthesized at 750 and 800 °C for 48 h have metastable β-Bi_2O_3 phase and this phase formed with the increase of synthesizing temperature.

Table II shows lattice parameters obtained using Diffrac Plus Eva software and Win-Index program of the stable samples having tetragonal β-Bi_2O_3 phase. As can be seen in Table II, the lattice parameters of A4 and A5 samples synthesized at 750 °C for 48 h decrease

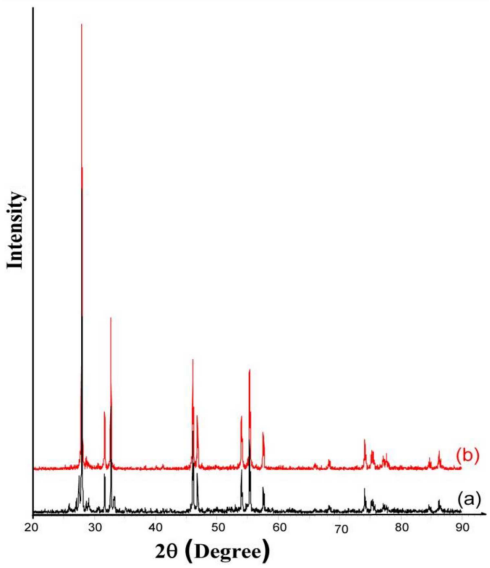

Fig. 1. XRD patterns of the A4 sample synthesized at (a) 700 °C and (b) 750 °C for 48 h.

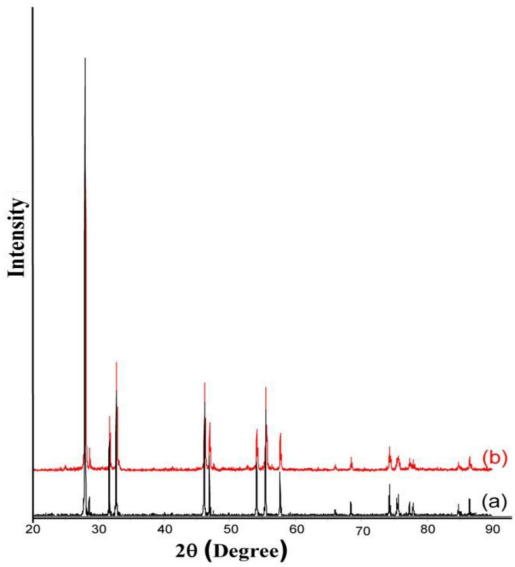

Fig. 2. XRD patterns of the A5 sample synthesized at (a) 750 °C and (b) 800 °C for 48 h.

TABLE I

Phase composition and doping amounts of the $(Bi_2O_3)_{1-x-y}(CeO_2)_x(Eu_2O_3)_y$ ternary system. x, y are in [mol%].

Synthesizing temperature [°C]	Synthesizing time [h]	A1	A2	A3	A4	A5	A6
		$x = 1$ $y = 11$	$x = 3$ $y = 9$	$x = 5$ $y = 7$	$x = 7$ $y = 5$	$x = 9$ $y = 3$	$x = 11$ $y = 1$
650	48	$\alpha+\beta+\gamma$	$\alpha+\beta+\gamma$	$\alpha+\beta+\gamma$	$\alpha+\beta+\gamma$	$\alpha+\beta+\gamma$	$\alpha+\beta+\gamma$
700	48	$\alpha+\beta+\gamma$	$\alpha+\beta+\gamma$	$\alpha+\beta+\gamma$	β	$\alpha+\beta+\gamma$	$\alpha+\beta+\gamma$
750	48	$\alpha+\beta+\gamma$	$\alpha+\beta+\gamma$	$\alpha+\beta+\gamma$	β	β	$\alpha+\beta+\gamma$
800	48	$\alpha+\beta+\gamma$	$\alpha+\beta+\gamma$	$\alpha+\beta+\gamma$	$\alpha+\beta+\gamma$	β	$\alpha+\beta+\gamma$

TABLE II

Doping amounts and lattice parameters of the $(Bi_2O_3)_{0.88}(CeO_2)_{0.07}(Eu_2O_3)_{0.05}$ and $(Bi_2O_3)_{0.88}(CeO_2)_{0.09}(Eu_2O_3)_{0.03}$ samples synthesized at 700, 750, and 800 °C for 48 h.

Samples	CeO_2 (x) [mol%]	Eu_2O_3 (y) [mol%]	Bi_2O_3 (1-x-y) [mol%]	Synthesizing temperature [°C]	Synthesizing time [h]	Phase	Lattice parameters		
							a [Å]	b [Å]	c [Å]
A4	7	5	88	700	48	β	7.7606	7.7606	5.6594
A4	7	5	88	750	48	β	7.7650	7.7650	5.6626
A5	9	3	88	750	48	β	7.7506	7.7506	5.6530
A5	9	3	88	800	48	β	7.7433	7.7433	5.6499

with increase of CeO_2 content. The lattice parameter, a-b and c, values of the samples in good agreement with tetragonal β-Bi_2O_3 phase obtained from XRD measurements and a-b and c values of the samples are in the range of 7.7433–7.7650 and 5.6499–5.6626 Å, respectively [17, 31].

3.2. Electrical conductivity measurements

We have carried out FPPT for the conductivity measurements of the samples having tetragonal β-phase, which have been performed within the temperature range of 100–800 °C. In Fig. 3, the electrical conductivity log σ curves of the A4 and A5 samples sintered at temperature range of 700–800 °C are given. As shown in this figure, all the curves are similar with each other. Conductivity values corresponding to different temperatures of stable samples were determined directly from Fig. 3.

The activation energies of the samples having β-Bi_2O_3 and their conductivity values corresponding to different temperatures which are directly from curves have been calculated from the Arrhenius equation

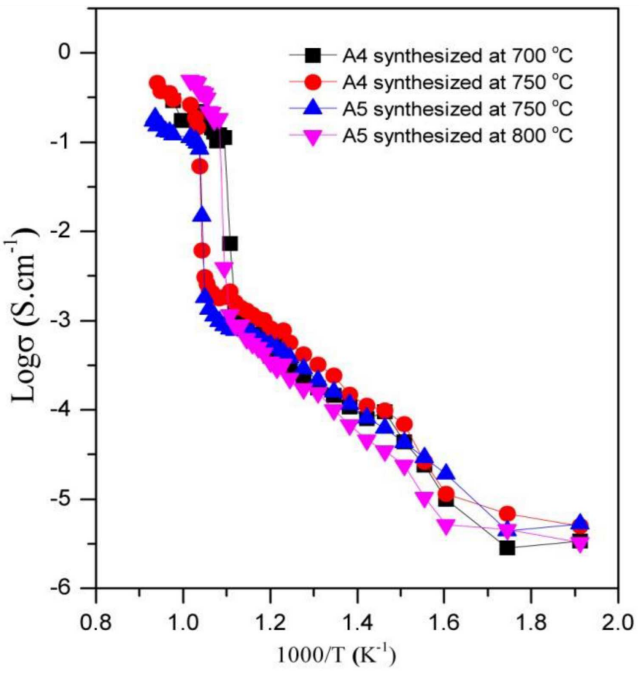

Fig. 3. The temperature dependence of electrical conductivities of the $(Bi_2O_3)_{0.88}(CeO_2)_{0.07}(Eu_2O_3)_{0.05}$ and $(Bi_2O_3)_{0.88}(CeO_2)_{0.09}(Eu_2O_3)_{0.03}$ samples synthesized at 700, 750, and 800 °C for 48 h.

$$\sigma = \sigma_0 \exp\left(-\frac{E_a}{k_B T}\right)$$

where σ_0 is the conductivity, T is the temperature in K, E_a is the activation energy of O^{2-} ions, k_B is the Boltzman constant (1.38×10^{-23} J/K).

We calculated the activation energies of the samples using a part of their conductivity curves with a constant slope and belonging to T_1 and T_2. The obtained conductivity values of the samples from their conductivity curves (Fig. 3) and their calculated activation energy values are given in Table III.

On the other hand, comparison of electrical conductivity was carried out for stable samples at the range of operating temperature of IT-SOFC, they are given in the last column in Table III. As expected, conductivities of the stable samples increase with decrease of activation energy values. All electrical conductivity values have similar characteristics as expected for solid ceramic materials based Bi_2O_3. As it can be seen in this table, A5 synthesized at 800 °C for 48 h has the best electrical conductivity and the highest conductivity value of this sample was measured as 4.76×10^{-1} S/cm at 700 °C. On the other hand, the A5 sample synthesized at 800 °C for 48 h has lowest activation energy value (0.7799 eV).

TABLE III

Electrical conductivities corresponding to T_1 and T_2, calculated activation energy values belonging to T_1 and T_2 of the samples $(Bi_2O_3)_{0.88}(CeO_2)_{0.09}(Eu_2O_3)_{0.03}$ synthesized at 700, 750 and 800 °C for 48 h and electrical conductivity at 700 °C of the stable samples.

Samples	CeO_2 (x) [mol%]	Eu_2O_3 (y) [mol%]	Bi_2O_3 (1-x-y) [mol%]	Synthesizing temperature [°C]	T_1-T_2 [K]	σ_1 [S/cm]	σ_2 [S/cm]	E_a [eV]	σ (700 °C) [S/cm]
A4	7	5	88	700	703–893	7.99×10^{-5}	1.34×10^{-3}	0.8040	2.08×10^{-1}
A4	7	5	88	750	703–813	1.12×10^{-4}	7.43×10^{-4}	0.8484	1.89×10^{-1}
A5	9	3	88	750	883–953	7.79×10^{-4}	1.81×10^{-3}	0.8746	1.05×10^{-1}
A5	9	3	88	800	663–873	2.38×10^{-5}	6.32×10^{-4}	0.7799	4.76×10^{-1}

3.3. Thermal analysis

Figure 4 shows the DTA and TGA curves of the A5 sample sintered in 750 °C for 48 h. As can be seen from DTA curve, exothermic peak on the cooling cycle and endothermic peak on the heating cycle are seen at 600 °C and 650 °C, respectively. At this temperature, there is a transition from tetragonal β-phase to cubic δ-phase according to the conductivity curve (Fig. 3). Therefore, it is seen that this result is confirmed when the conductivity curves are compared with each other. During examination of electrical conductivity curve of this sample, it can be seen that the conductivity has increased up by nearly two orders of magnitude at 650 °C as the temperature increases.

The TGA curve of the A5 sample sintered in 750 °C for 48 h shows that there is no mass loss during the heating and cooling process.

Figure 5 shows DTA and TGA curves of the A5 sample sintered at 800 °C for 48 h. As can be seen in Fig. 5, DTA curve of this sample has similar characteristics with DTA curve of A5 sample sintered in 750 °C for 48 h (Fig. 4). An exothermic peak on the cooling cycle and endothermic peak on the heating cycle are seen at 600 °C and 650 °C, respectively. At this temperature, there is a transition from tetragonal β-phase to cubic δ-phase according to the conductivity curve (Fig. 3). As can be seen from TGA curve of this sample, there is almost no weight loss during the heating and cooling treatment processes.

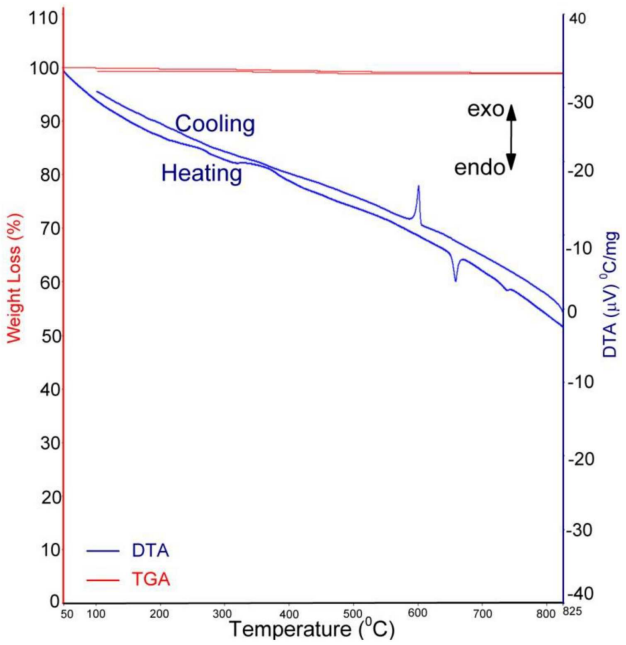

Fig. 4. DTA/TGA curves of sample $(Bi_2O_3)_{0.88}(CeO_2)_{0.09}(Eu_2O_3)_{0.03}$ sintered at 750 °C for 48 h.

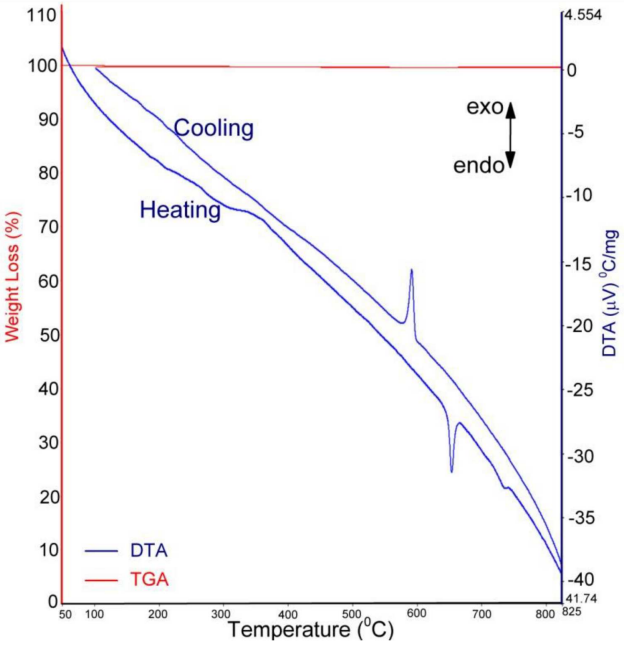

Fig. 5. As in Fig. 4 but at 800 °C.

4. Conclusions

In this work, 24 $(Bi_2O_3)_{1-x-y}(CeO_2)_x(Eu_2O_3)_y$ ternary system samples with different percentages (x = 0.01, 0.03, 0.05, 0.07, 0.09, 0.11 and y = 0.11, 0.09, 0.07, 0.05, 0.03, 0.01 dopant concentrations) keeping the percentage of the Bi_2O_3 constant (0.88%) were fabricated by the SST sintering at 650, 700, 750, and 800 °C for 48 h. Characterization of the samples was performed by XRD, FPPT, DTA, and TGA measurements. According to the XRD results, two samples in A4 group (x = 0.07 and y = 0.05) sintered at 700, 750 °C and two samples in A5 group (x = 0.09 and y = 0.03) sintered at 750, 800 °C have tetragonal β-phase. It was also observed that the lattice parameters of the $(Bi_2O_3)_{0.88}(CeO_2)_{0.07}(Eu_2O_3)_{0.05}$ and $(Bi_2O_3)_{0.88}(CeO_2)_{0.09}(Eu_2O_3)_{0.03}$ samples synthesized at 750 °C for 48 h decreased with increase of CeO_2 content. FPPT measurements have shown that the measured ionic conductivity of the stable samples vary in the range 1.05×10^{-1}–4.76×10^{-1} S/cm. On the other hand, it was found that there is a good correlation between the activation energy values (0.7799–0.8746 eV) and conductivity values. DTA and TGA measurements showed that there is a good correlation between the endothermic and exothermic reactions and the phase transitions.

As a result, electrolyte samples having stable structure fabricated by us, after carrying out long-term tests of durability and efficiency, can be used for SOFCs.

Acknowledgments

This work was funded by Nigde University Research Projects Unit under the grant no. FEB 2008/09.

References

[1] A. Brisse, J. Schefold, M. Zahid, *Int. J. Hydrogen En.* **33**, 5375 (2008).

[2] K.T. Lee, D.W. Jung, M.A. Camaratta, H.S. Yoon, J.S. Ahn, E.D. Wachsmani, *J. Power Sources* **205**, 122 (2012).

[3] X. Liu, H. Fan, J. Shi, G. Dong, Q. Li, *Int. J. Hydrogen. En.* **39**, 17819 (2014).

[4] D.S. Khaerudini, G. Guan, P. Zhang, X. Hao, Y. Kasai, K. Kusakabe, A. Abudula, *J. Alloys Comp.* **589**, 29 (2014).

[5] E.W. Bohannan, C.C. Jaynes, M.G. Shumsky, J.K. Barton, J.A. Switzer, *Solid State Ion.* **131**, 97 (2000).

[6] M.L. Tate, J. Hack, X. Kuang, G.J. McIntyre, R.L. Withers, M.R. Johnson, I. Radosavljevic Evans, *J. Solid State Chem.* **225**, 383 (2015).

[7] H. Kishimotoa, K. Yashiro, T. Shimonosono, M.E. Brito, K. Yamaji, T. Horita, H. Yokokawa, J. Mizusaki, *Electrochim. Acta* **82**, 263 (2012).

[8] B. Timurkutluk, S. Celik, C. Timurkutluk, M.D. Mat, Y. Kaplan, *Int. J. Hydrogen En.* **37**, 3499 (2012).

[9] N.A.S. Webster, C.D. Ling, C.L. Raston, F.J. Lincoln, *Solid State Ion.* **178**, 1451 (2007).

[10] M.Y. Tan, K.B. Tan, Z. Zainal, C.C. Khaw, S.K. Chen, *Ceram. Int.* **38**, 3403 (2012).

[11] N.M. Sammes, G.A. Tompsett, H. Nafe, F. Aldinger, *J. Eur. Ceram. Soc.* **19**, 1801 (1999).

[12] A.J. Jacobson, *Chem. Mater.* **22**, 660 (2010).

[13] G. Corbel, E. Chevereau, S. Kodjikian, P. Lacorre, *Inorg. Chem.* **46**, 6395 (2007).

[14] A.L.J. Pereira, O. Gomis, J.A. Sans, J. Pellicer-Porres, F.J. Manjón, A. Beltran, P. Rodríguez-Hernandez, A. Muñoz, *J. Phys. Condens. Matter* **26**, 225401 (2014).

[15] N. Jiang, E.D. Wachsman, S.H. Jung, *Solid State Ion.* **150**, 347 (2002).

[16] M. Leszczynska, M. Holdynski, F. Krok, I. Abrahams, X. Liu, W. Wrobel, *Solid State Ion.* **181**, 796 (2010).

[17] A. Dapčević, D. Poleti, J. Rogan, A. Radojković, M. Radović, G. Branković, *Solid State Ion.* **280**, 18 (2015).

[18] T.M. Gesing, R.X. Fischer, M. Burianek, M. Mühlberg, T. Debnath, C.H. Rüscher, J. Ottinger, J.C. Buhl, H. Schneider, *J. Eur. Ceram. Soc.* **31**, 3055 (2011).

[19] G. Corbel, E. Suard, P. Lacorre, *Chem. Mater.* **23**, 1288 (2011).

[20] V. Sadykov, N. Mezentseva, M. Arapova, T. Krieger, E. Gerasimov, G. Alikina, V. Pelipenko, A. Bobin, V. Muzykantov, Y. Fedorova, E. Sadovskaya, N. Eremeev, V. Belyaev, Y. Okhlupin, N. Uvarov, *Solid State Ion.* **251**, 34 (2013).

[21] K. Brinkman, T. Iijima, H. Takamura, *Solid State Ion.* **181**, 53 (2010).

[22] S. Boyapati, E.D. Wachsman, N. Jiang, *Solid State Ion.* **140**, 149 (2001).

[23] T.B. Tran, A. Navrotsky, *Chem. Mater.* **24**, 4185 (2012).

[24] G. Singla, P.K. Jha, J. Kaur-Gill, K. Singh, *Ceram. Int.* **38**, 2065 (2012).

[25] R. Li, Q. Zhena, M. Drache, A. Rubbens, R.N. Vannier, *J. Alloys Comp.* **494**, 446 (2010).

[26] S.E. Lin, W.C.J. Wei, *J. Eur. Ceram. Soc.* **31**, 3081 (2011).

[27] D.S. Khaerudini, G. Guan, P. Zhang, X. Hao, Y. Kasai, K. Kusakabe, A. Abudula, *J. Alloys Comp.* **589**, 29 (2014).

[28] S. Arasteh, A. Maghsoudipour, M. Alizadeh, A. Nemati, *Ceram. Int.* **37**, 3451 (2011).

[29] H. Katayama, S. Tamura, N. Imanaka, *Solid State Ion.* **192**, 134 (2011).

[30] C.Y. Hsieh, H.S. Wang, K.Z. Fung, *J. Eur. Ceram. Soc.* **31**, 3073 (2011).

[31] L. Bourja, B. Bakiz, A. Benlhachemi, M. Ezahri, S. Villain, O. Crosnier, C. Favotto, J.R. Gavarri, *J. Solid State Chem.* **184**, 608 (2011).